Enhancement of magnon-magnon entanglement inside a cavity

H. Y. Yuan,[1,*] Shasha Zheng,[2,3,4] Zbigniew Ficek,[5] Q. Y. He,[2,3,4,†] and Man-Hong Yung[6,7,8,‡]

[1]*Department of Physics, Southern University of Science and Technology, Shenzhen 518055, China*

[2]*State Key Laboratory for Mesoscopic Physics, School of Physicsand Frontiers Science Center for Nano-optoelectronics, Peking University, Beijing 100871, China*

[3]*Beijing Academy of Quantum Information Sciences, Haidian District, Beijing 100193, China*

[4]*Collaborative Innovation Center of Extreme Optics, Shanxi University, Taiyuan, Shanxi 030006, China*

[5]*Quantum Optics and Engineering Division, Institute of Physics, University of Zielona Góra, Zielona Góra, Poland*

[6]*Institute for Quantum Science and Engineering and Department of Physics, Southern University of Science and Technology, Shenzhen 518055, China*

[7]*Shenzhen Key Laboratory of Quantum Science and Engineering, Shenzhen 518055, China*

[8]*Central Research Institute, Huawei Technologies, Shenzhen 518129, China*

(Received 20 April 2019; revised manuscript received 21 October 2019; published 14 January 2020)

Magnon-photon coupling inside a cavity has been experimentally realized and has attracted significant attention for its potential docking with quantum information science. Whether this coupling implies the steady entanglement of photons and magnons is crucial for its usage in quantum information but is still an open question. Here we study the entanglement properties among magnons and photons in an antiferromagnet-light system and find that the entanglement between a magnon and a photon is nearly zero, while the magnon-magnon entanglement is very strong and can be even further enhanced through the coupling with the cavity photons. The maximum enhancement occurs when the antiferromagnet is resonant with the light. The essential physics can be well understood within the picture of cavity-induced cooling of the magnon-magnon state near its joint vacuum with stronger entanglement. Our findings can be used to cool magnetic magnons toward their ground state and may also be significant to extend the cavity spintronics to quantum manipulation. Furthermore, the hybrid antiferromagnet-light system provides a natural platform to manipulate the deep strong correlations of continuous modes with a generic stable condition and easy tunability.

DOI: 10.1103/PhysRevB.101.014419

I. INTRODUCTION

Antiferromagnetic (AFM) spintronics has gained interest because of its better stability and fast dynamics over its ferromagnetic counterpart [1,2]. Of particular interest are antiferromagnetic spin waves (magnons) that show much richer physics than ferromagnets, such as the spin pumping at the interface of an AFM/normal-metal bilayer [3], magnon spin current enhancement through an AFM layer [4–7], long-distance magnon transport [8–10], and magnon-driven magnetic structure motion [11–13]. It was recently theoretically proposed [14] and experimentally demonstrated [15–17] that antiferromagnetic magnons can be strongly coupled to the light by placing an AFM element into a cavity. The observed coupling spectrum takes on energy level repulsion near resonance, while the coupling strength (the energy gap at zero detuning) is proportional to the square root of the number of spins [14,15]. The magnon-photon hybrid state (magnon-polariton) not only provides a promising platform to study the fundamental physics of the macroscopic quantum state [18] but also shows promising applications in quantum information science and engineering, such as quantum transducers, sensors, and memories [19–22]. Furthermore, the integration of the magnon-polariton with quantum qubits may enable the precise control and readout of magnetic excitations [23,24].

Most studies on magnon-polariton hybrid systems have focused on the determination of the coupling spectrum of the magnon-polariton, which can be well described by the classical harmonic oscillator model [25]. A little work has been done on the quantum correlations among magnons and photons, especially their entanglement properties. This issue becomes important when the magnon-polariton reaches the quantum regime at low temperature and may further manifest its role if it is intended to be used as a solid-state entanglement source for quantum tasks such as quantum channel discrimination [26].

Interesting theoretical and experimental studies have also been carried out for strongly coupled magnon and photon modes in ferromagnets and ferrimagnets, where reversible long-lived magnon-photon entangled states may be generated [27–32]. The theoretical calculations performed are essentially equivalent to those of the Tavis-Cummings model [33–37] in that the ferromagnetic spin wave (magnon) interacts strongly with a single-mode cavity in the absence of

*huaiyangyuan@gmail.com
†qiongyihe@pku.edu.cn
‡yung@sustech.edu.cn

dissipation. In this reversible system the magnon is coupled to the cavity mode through the beam-splitter-type interaction [27,28,38–40]. In this case, the generated magnon-photon entangled state results from the coherent exchange of excitation between the magnon and cavity-photon states and, due to the strong coupling, may exhibit long-lived Rabi oscillations.

Other studies on magnon-photon entanglement have been carried out for dissipative (irreversible) three-mode magnon-photon-phonon systems in which the nonlinear interaction between these modes produces steady-state entanglement between irreversibly decaying modes [41]. It has also been shown that two magnons can be entangled through their simultaneous interaction with cavity photons [21,42]. More interestingly, the magnon and photon could form a stationary Bell state through a dissipative beam-splitter-type interaction [43]. Recently, a proof-of-principle experiment established the use of the hybrid magnon-photon system as a single-magnon detector [40].

In this paper, we study the steady-state entanglement properties among magnons and photons in an AFM-light system. Here, the coupling configuration between the modes is markedly different from those present, for example, in ferromagnets. In the AFM, the two types of magnons are mutually coupled to each other through a parametric-type interaction and are coupled through a beam-splitter-type interaction and parametric-type interaction to the photon mode. In addition, the modes decay with nonzero decay rates resulting from the coupling of the modes to an external noise environment. We find that these couplings lead to steady-state magnon-photon entanglement which is very weak near the anticrossing point of the spectrum. However, the magnon-magnon entanglement is found to be very strong at this anticrossing point and can even be significantly stronger than those in the absence of light. We explain these entanglement properties as resulting from the deep strong coupling between the magnons. We use the cavity-cooling picture to explain the essential physics of the process which is behind the enhancement of the entanglement, that the cavity photons effectively cool the magnons toward their vacuum state. This physical principle can be further interpreted as the entanglement evolution of a system with distinguished correlation properties of its ground state and excited state and thus naturally gives a unified understanding of the anomalous entanglement change in the literature [44,45]. Our results explore further the entangled nature of antiferromagnetic magnons and thus allow us to understand better the properties of antiferromagnets as well as magnon-magnon correlations. In addition, these results provide a simple picture of how to cool magnetic magnons toward their ground state with the assistance of cavity photons. Besides the importance to quantify the entanglement between magnons and photons, the determination of magnon-magnon entanglement also becomes essential for the fundamental interest in the macroscopic quantum effect and may have a potential application as a solid source for quantum science and technologies. Furthermore, our finding may be significant if one tends to use the hybrid magnon-photon state in various quantum tasks, such as quantum communication, computation, and information science, where the entanglement among magnons is an important resource.

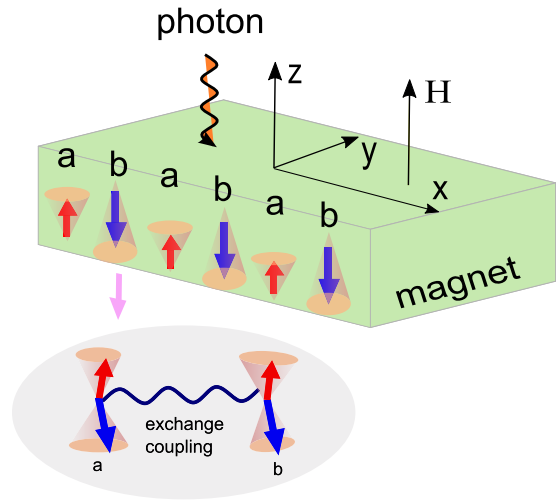

FIG. 1. Scheme of a two-sublattice ferrimagnet and its coupling with an electromagnetic wave. The magnetic moments on the two sublattices (red and blue arrows) pointing along $\pm z$ directions represent the classical ground state of the system. The bottom panel indicates the existence of magnon-magnon coupling.

II. GENERAL FORMALISM

We begin with a description of a general theory of the magnet-light interaction in a two-sublattice magnet, as illustrated in Fig. 1. We concentrate on the AFM case followed by a brief discussion on ferrimagnetic (FiM) and ferromagnetic (FM) cases. The Hamiltonian of a magnet coupled to a microwave field inside a cavity through its magnetic field component can be written as $\mathcal{H} = \mathcal{H}_{\rm FiM} + \mathcal{H}_{\rm ph} + \mathcal{H}_{\rm int}$, where $\mathcal{H}_{\rm FiM}$, $\mathcal{H}_{\rm ph}$, and $\mathcal{H}_{\rm int}$ are, respectively, the Hamiltonians for the FiM, photon, and their interaction and read

$$\begin{aligned}\mathcal{H}_{\rm FiM} &= J\sum_{l,\delta}\mathbf{S}_l\cdot\mathbf{S}_{l+\delta} - \sum_l(\mathbf{H}+\mathbf{H}_{\rm an})\cdot\mathbf{S}_l,\\ \mathcal{H}_{\rm ph} &= \frac{1}{2}\int\left(\epsilon_0\mathbf{E}_f^2 + \frac{1}{\mu_0}\mathbf{B}_f^2\right)dxdydz,\\ \mathcal{H}_{\rm int} &= -\sum_l\mathbf{S}_l\cdot\mathbf{H}_f,\end{aligned} \tag{1}$$

where $J > 0$ is the exchange constant; $\mathbf{S}_l$ is the spin on site l; δ is the displacement of the two nearest spins; $\mathbf{H}$ and $\mathbf{H}_{\rm an}$ are the external static and anisotropy fields, respectively; $\mathbf{E}_f$ and $\mathbf{B}_f$ are electric field and magnetic inductance components of the electromagnetic (EM) wave; $\mathbf{H}_f$ is the corresponding magnetic field; and ϵ_0 and μ_0 are, respectively, vacuum permittivity and susceptibility. Note that $\mathbf{H}_f$ is time dependent and it drives the dynamics of the whole system.

Using the Holstein-Primakoff transformation [46]

$$\begin{aligned}S_i^{+,a} &= \sqrt{2S_a}a_i,\ S_i^{+,b} = \sqrt{2S_b}b_i^\dagger,\\ S_i^{-,a} &= \sqrt{2S_a}a_i^\dagger,\ S_i^{-,b} = \sqrt{2S_b}b_i,\\ S_i^{z,a} &= S_a - a_i^\dagger a_i,\ S_i^{z,b} = b_i^\dagger b_i - S_b,\end{aligned} \tag{2}$$

where $S_i^{\pm,\mu} = S_i^{x,\mu} \pm iS_i^{y,\mu}$ are the spin raising and lowering operators and a_i, b_i, and $(a_i^\dagger, b_i^\dagger)$ are the magnon annihilation

(creation) operators on the ith site, the $\mathcal{H}_{\rm FiM}$ Hamiltonian can be written as

$$\mathcal{H}_{\rm FiM} = \sum_q [\omega_a a_q^\dagger a_q + \omega_b b_q^\dagger b_q + g_{ab}(a_q^\dagger b_q^\dagger + a_q b_q)], \quad (3)$$

where $\omega_a = H_{\rm ex,b} + H_{\rm an,a} + H$, $\omega_b = H_{\rm ex,a} + H_{\rm an,b} - H$, $H_{{\rm ex},\mu} = 2zJS_\mu^2$ ($\mu = a, b$), S_μ is the magnitude of spin vector, z is the coordination number, and $g_{ab} = \sqrt{H_{\rm ex,a}H_{\rm ex,b}}\cos(q\delta)$ is the coupling constant of magnon modes excited on the two sublattices. In Eq. (3), $a_q^\dagger$ and $b_q^\dagger$ (a_q and b_q) are the creation (annihilation) operators of the magnons on the two sublattices with wave vector q, which satisfy the standard commutation relations for bosons. In the interaction part of the Hamiltonian (3), we keep terms to second order in the coupling strength; the higher-order terms involving four or more magnon operators have been neglected because their excitation probabilities are typically very small when the temperature of the system is far below the Néel temperature, as considered here.

It should be noted that the Hamiltonian (3) is obtained without using the rotating-wave approximation because the coupling constant between the magnons g_{ab} is of the order of the frequencies ω_a and ω_a. This strong coupling, leading to the parametric-type coupling between the two magnons $(a^\dagger b^\dagger + ab)$, results from the antiferromagnetic nature of the system, where the spin reduction in sublattice a (b) is always accompanied by spin increasing in sublattice b (a). This makes the antiferromagnet system different from a large class of multimode systems considered in the weak-coupling regime, where the beam-splitter-type terms play a dominate role in the rotating-wave approximation. The parametric-type terms are usually omitted as these terms are accompanied by the fast-oscillating terms, which average to zero over a long evolution time.

Further, a circularly polarized EM wave can be quantized as $\mathcal{H}_{\rm ph} = \sum_q \omega_c c_q^\dagger c_q$, where $c_q^\dagger$ (c_q) is the creation (annihilation) operator of the quantized EM mode with wave vector q and ω_c is its frequency [47]. Next, by substituting the quantized form of the oscillating magnetic field, $\mathbf{H}_f = i\sqrt{\mu_0\omega_q/4V}\sum_q \mathbf{q}\times[\mathbf{u}(\mathbf{q})c_q e^{i\mathbf{q}\cdot\mathbf{r}} - \mathbf{u}^*(\mathbf{q})c_q^\dagger e^{-i\mathbf{q}\cdot\mathbf{r}}]$, into $\mathcal{H}_{\rm int}$, the resulting interaction term between the magnons and the photon field becomes $\mathcal{H}_{\rm int} = \sum_q [g_{ac}(a_q^\dagger c_q^\dagger + a_q c_q) + g_{bc}(b_q^\dagger c_q + b_q c_q^\dagger)]$, where $g_{\mu c} = \sqrt{\mu_0\omega_c S_\mu N/2V}$, with $\mu = a, b$ being the interaction constant between the magnon μ and the photon mode c [14], and N and V are the number of spins on each sublattice and the volume of the cavity. Hence, the total Hamiltonian can be written as

$$\begin{aligned}\mathcal{H} = &\sum_q [\omega_a a_q^\dagger a_q + \omega_b b_q^\dagger b_q + g_{ab}(a_q^\dagger b_q^\dagger + a_q b_q)] \\ &+ \sum_q [\omega_c c_q^\dagger c_q + g_{ac}(a_q^\dagger c_q^\dagger + a_q c_q) + g_{bc}(b_q^\dagger c_q + b_q c_q^\dagger)].\end{aligned} \quad (4)$$

Note that the two types of magnons are coupled with photons in different ways. This is because the angular momentum conservation principle implies that circularly polarized light can interact with only one type of magnon through the particle-conserving process (beam-splitter-type interaction) while the other type of magnon can be excited only without conserving the particle number. If we use elliptical or linearly polarized light, the Hamiltonian will be different, but the essential physics presented below are similar.

To proceed further note that the slope of the photon dispersion is much steeper than that of the magnon; hence, the photon can couple with the magnon only around $q = 0$, i.e., the magnetic resonance mode. Therefore, for simplicity, we treat $q = 0$ such that the sum in Hamiltonian (1) can be removed and $g_{ab} = \sqrt{H_{\rm ex,a}H_{\rm ex,b}}$. From now on, we also eliminate the subscript q for expression simplicity; then the resultant Hamiltonian reads

$$\begin{aligned}\mathcal{H} = &\omega_a a^\dagger a + \omega_b b^\dagger b + g_{ab}(a^\dagger b^\dagger + ab) \\ &+ \omega_c c^\dagger c + g_{ac}(a^\dagger c^\dagger + ac) + g_{bc}(b^\dagger c + bc^\dagger),\end{aligned} \quad (5)$$

in which $g_{ab} = \sqrt{H_{\rm ex,a}H_{\rm ex,b}}$ is the coupling constant between magnon modes excited on the two sublattices and $a^\dagger$, $b^\dagger$, and $c^\dagger$ (a, b, and c) refer to the creation (annihilation) operators for magnons corresponding to the uniform precession mode and photons, respectively.

The Hamiltonian (5) leads to the quantum Langevin equations,

$$\begin{aligned}\frac{da}{dt} &= -(\gamma_a + i\omega_a)a - ig_{ab}b^\dagger - ig_{ac}c^\dagger + \sqrt{2\gamma_a}a_{\rm in}, \\ \frac{db}{dt} &= -(\gamma_b + i\omega_b)b - ig_{ab}a^\dagger - ig_{bc}c + \sqrt{2\gamma_b}b_{\rm in}, \\ \frac{dc}{dt} &= -(\gamma_c + i\omega_c)c - ig_{ac}a^\dagger - ig_{bc}b + \sqrt{2\gamma_c}c_{\rm in},\end{aligned} \quad (6)$$

where, in accordance with the standard fluctuation-dissipation theorem [47], we have included dissipation terms; γ_a, γ_b, and γ_c are the damping rates of the modes, and $a_{\rm in}$, $b_{\rm in}$, and $c_{\rm in}$ are input quantum noises for each mode. We will assume the Gaussian nature of the input noises [48], which have zero mean average and a δ correlation in the form of $\langle a_{\rm in}(t)a_{\rm in}^\dagger(t')\rangle = \langle b_{\rm in}(t)b_{\rm in}^\dagger(t')\rangle = \langle c_{\rm in}(t)c_{\rm in}^\dagger(t')\rangle = \delta(t-t')$.

To quantify the entanglement of two arbitrary modes in the system, we introduce the quadrature components of the field operators of each mode as $X_\mu = (\mu + \mu^\dagger)/\sqrt{2}$ and $Y_\mu = (\mu - \mu^\dagger)/\sqrt{2}i$ ($\mu = a, b, c$). Then, introducing a vector $\mathbf{u} = (X_a, Y_a, X_b, Y_b, X_c, Y_c)^T$ for the quadrature components, we can put the Langevin equation (6) into matrix form,

$$d\mathbf{u}/dt = \bar{\mathbf{M}}\mathbf{u} + \Lambda\mathbf{u}_{\rm in}, \quad (7)$$

where $\bar{\mathbf{M}}$ is the drift matrix,

$$\bar{\mathbf{M}} = \begin{pmatrix} -\gamma_a & \omega_a & 0 & -g_{ab} & 0 & -g_{ac} \\ -\omega_a & -\gamma_a & -g_{ab} & 0 & -g_{ac} & 0 \\ 0 & -g_{ab} & -\gamma_b & \omega_b & 0 & g_{bc} \\ -g_{ab} & 0 & -\omega_b & -\gamma_b & -g_{bc} & 0 \\ 0 & -g_{ac} & 0 & g_{bc} & -\gamma_c & \omega_c \\ -g_{ac} & 0 & -g_{bc} & 0 & -\omega_c & -\gamma_c \end{pmatrix}, \quad (8)$$

$\mathbf{u}_{\rm in} = (X_{\rm in,a}, Y_{\rm in,a}, X_{\rm in,b}, Y_{\rm in,b}, X_{\rm in,c}, Y_{\rm in,c})^T$, and $\Lambda = {\rm diag}(\sqrt{2\gamma_a}, \sqrt{2\gamma_a}, \sqrt{2\gamma_b}, \sqrt{2\gamma_b}, \sqrt{2\gamma_c}, \sqrt{2\gamma_c})$.

The linearity of the Langevin equation together with the Gaussian nature of the noise implies that the modes will decay to a stationary Gaussian state, which can be fully characterized by a stationary covariance matrix $\mathbf{V}$ defined as $V_{ij} = \langle u_i u_j + u_j u_i\rangle/2$. The matrix $\mathbf{V}$ is obtained by solv-

ing the Lyapunov equation [49], $\bar{\mathbf{M}}\mathbf{V} + \mathbf{V}\bar{\mathbf{M}}^T = -\mathbf{D}$, where $\mathbf{D} = \mathrm{diag}(\gamma_a, \gamma_a, \gamma_b, \gamma_b, \gamma_c, \gamma_c)$. The stability of the stationary state will be checked using the Routh-Hurwitz criterion [50]. According to the criterion, the system is stable if all the eigenvalues of $\bar{\mathbf{M}}$ have negative real parts, which, as we shall see, is almost automatically satisfied for an AFM.

In terms of the covariance matrix, the degree of entanglement between two modes of interest can be quantified by the logarithmic negativity defined as $E_N = \max[0, -\ln[2\eta^-]]$, where $\eta^- = \sqrt{\sum(\mathbf{V}') - [\sum \mathbf{V}'^2 - 4\det \mathbf{V}']^{1/2}}/\sqrt{2}$, with $\sum \mathbf{V}'$ and $\det \mathbf{V}'$ being the two symplectic invariants of the reduced covariance matrix $\mathbf{V}'$ of two modes [51,52] (see Appendix A for the calculation of the two symplectic invariants).

III. ANTIFERROMAGNETIC MAGNON-MAGNON ENTANGLEMENT

In an AFM, the sublattice permutation symmetry implies $S_a = S_b \equiv S$, $\gamma_a = \gamma_b \equiv \gamma_m$, $g_{ab} = H_{\mathrm{ex}} \equiv 2zJS^2$, $g_{ac} = g_{bc} \equiv g_{\mathrm{mp}}$. In this case, we can analytically solve the eigenequation $\det(\lambda\mathbf{I} - \bar{\mathbf{M}}) = 0$ and obtain $\lambda_{1,2,3,4} = -\gamma_m - i(H_{\mathrm{sp}} \pm H)$ for $g_{\mathrm{mp}} = 0$, where each eigenvalue is doubly degenerate and $H_{\mathrm{sp}} = \sqrt{H_{\mathrm{an}}(H_{\mathrm{an}} + 2H_{\mathrm{ex}})}$ is a spin-flop field of the system. Since the dissipation rate $\gamma_m > 0$, the system can always reach a stable steady state, regardless of the initial states. This stability condition imposes fewer constraints on the parameters than those in the traditional three-mode optomechanical systems, where strict constraints on the coupling strengths and the dissipation rates are required [53]. This conclusion is also valid in the case of $g_{\mathrm{mp}} \neq 0$ (see Appendix B for the discussion of the stability regime of the magnet-light system).

Figure 2(a) shows that the magnon-photon entanglement is zero (dot-dashed line at $E_N = 0$), while the magnon-magnon entanglement is significantly enhanced compared with the value in the absence of light (dashed line around $\ln 2$; see Appendix A for a detailed calculation of this value). As the photon frequency is tuned from $\omega_c/H_{\mathrm{sp}} = 0.80$ (black) to 0.85 (red) to 0.90 (blue), the maximum enhancement locates at $H/H_{\mathrm{sp}} = 0.20$, 0.15, and 0.10, respectively. To analyze the essential physics, we first diagonalize the antiferromagnetic Hamiltonian $\mathcal{H}_{\mathrm{FiM}}$ in Eq. (1) by introducing two Bogoliubov modes $\alpha = \cosh\theta a - \sinh\theta b^\dagger$, $\beta = -\sinh\theta a^\dagger + \cosh\theta b$, where $\tanh 2\theta = -2g_{ab}/(\omega_a + \omega_b)$. In terms of the Bogoliubov modes, the Hamiltonian (5) becomes

$$\mathcal{H} = \omega_\alpha \alpha^\dagger\alpha + \omega_\beta\beta^\dagger\beta + \omega_c c^\dagger c + g_{\alpha c}(\alpha^\dagger c^\dagger + \alpha c) + g_{\beta c}(\beta c^\dagger + \beta^\dagger c), \quad (9)$$

where $g_{\alpha c} = g_{ac}\cosh\theta + g_{bc}\sinh\theta$, $g_{\beta c} = g_{ac}\sinh\theta + g_{bc}\cosh\theta$, and $\omega_{\alpha,\beta} = \pm H + H_{\mathrm{sp}}$ represent the optical and acoustic magnon bands, respectively.

Let us first analyze the position of maximum enhancement of magnon-magnon entanglement in the presence of photons. The two eigenmodes of magnons $\omega_{\alpha,\beta}$ together with the photon mode for $\omega_c/H_{\mathrm{sp}} = 0.85$ are plotted in Fig. 2(b) as dashed lines. Now we immediately see that the maximum enhancement of entanglement, as seen in Fig. 2(a), appears when the strong coupling occurs by adjusting the external field $H/H_{\mathrm{sp}} = 0.15$ so that the photon frequency becomes

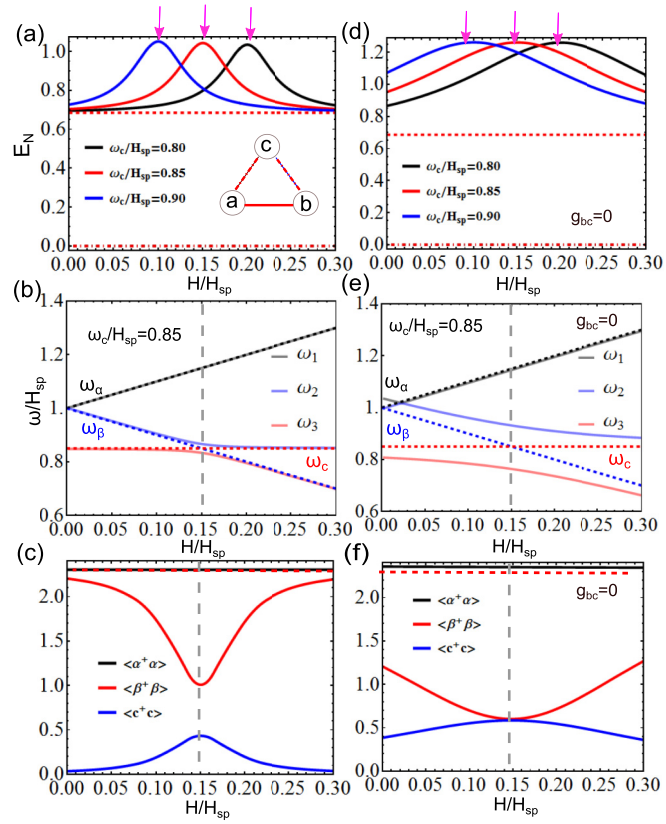

FIG. 2. (a) The enhanced entanglement E_N between two magnons a and b in the presence of light mode c as a function of external field H/H_{sp} for photon frequency $\omega_c/H_{\mathrm{sp}} = 0.80$ (black line), 0.85 (red line), 0.90 (blue line). The horizontal dashed line at $E_N = 0.6851$ is the magnon-magnon entanglement without light, while the dot-dashed line at $E_N = 0$ indicates no entanglement between $a - c$ and $b - c$. (b) The dispersion relations for an antiferromagnet with $\omega_c/H_{\mathrm{sp}} = 0.85$ and $g_{ac} = g_{bc} = 0.01H_{\mathrm{ex}}$. Obviously, the optical magnon band ω_α is left unchanged, while the acoustic band ω_β is hybridized with the photon mode ω_c to form modes $\omega_{2,3}$. (c) The population of modes c and α, β. The red dashed line represents the occupation of α/β mode without light. (d)–(f) The same as (a)–(c), but with $g_{ac} = 0.01H_{\mathrm{ex}}$ and $g_{bc} = 0$. Other parameters are $g_{ab} = H_{\mathrm{ex}}$, $H_{\mathrm{an}} = 0.0163H_{\mathrm{ex}}$, $\gamma_{\mathrm{m}} = 0.001H_{\mathrm{ex}}$, and $\gamma_c = 0.003H_{\mathrm{ex}}$. For simplicity in the following all the parameters are expressed in units of H_{ex}.

resonant with the frequency of the acoustic magnon β, i.e., $\omega_\beta = \omega_c$. Due to the coupling of magnons with photons, a gap should open near the crossing point $H/H_{\mathrm{sp}} = 0.15$, as shown by solid blue and red lines in Fig. 2(b); that is, the eigenmodes $\omega_{1,2,3}$ of the coupled system become superpositions of the magnon modes and photon mode. Here, acoustic magnon frequency ω_β and photon frequency ω_c superpose to form the eigenfrequencies ω_2 and ω_3, while the optical magnon mode ω_α is left unchanged as a dark mode [14], indicated by $\omega_1 = \omega_\alpha$ [merged black dashed line and gray solid line in Fig. 2(b)]. The depth of the anticrossing gap at $H/H_{\mathrm{sp}} = 0.15$ indicates the effective coupling strength between magnons and photons.

We now proceed to explain the enhancement of the magnon-magnon entanglement in the presence of the light mode. In terms of the two-mode squeezing operator $S(\theta) =$

$\exp[\theta(ab - a^\dagger b^\dagger)]$ [54], the magnon eigenmodes can be reformulated as $\alpha = S(\theta)aS^\dagger(\theta)$, $\beta = S(\theta)bS^\dagger(\theta)$, and thus, the joint ground state of the α and β modes is a two-mode squeezed state $|\theta\rangle = S(\theta)|0_a, 0_b\rangle$ with entanglement $2|\theta|$ (see Appendix C for the calculation of the entanglement of a two-mode squeezed state), where $|0_a, 0_b\rangle$ is the joint vacuum of magnon modes a and b. According to Eq. (9), the photon mode couples with the acoustic magnon mode β by a beam-splitter-type interaction and thus serves as a cooling bath to cool the mode β toward its ground state [55]. Note that the ground-state entanglement $E_N = 2|\theta| \approx \text{arctanh}(1 + H_{\text{an}}/H_{\text{ex}})^{-1} \approx 2.41$ is larger than the entanglement in the absence of the light ($\ln 2$). This cooling mechanism consequently enhances the entanglement of two magnons. As the other Bogoliubov mode α is a dark mode that is nonresonant with the photons, its role in the cooling process can thus be neglected. To demonstrate this point, we plot the average population of α, β, and c in Fig. 2(c) as black, red, and blue lines, respectively. Clearly, the occupancy of mode β is reduced towards its ground state under cavity cooling and takes on the minimum, while the population of the photon mode c takes on a maximum near the anticrossing point, where the strong coupling between β and c occurs and the cooling effect is most efficient. The population of the dark mode α is almost unchanged when we tune the field, as it is decoupled from the cavity mode c. This means that the achieved state is not an ideal two-mode squeezed vacuum state as α is not cooled, but Fig. 2(a) shows that the entanglement is significantly enhanced $E_N \approx 1.05$.

To further testify the presence of cavity cooling, we artificially tune $g_{bc} = 0$ and find that the magnon-magnon enhancement becomes even stronger, as shown in Fig. 2(d). This is because the coupling strength $|g_{\beta c}|$ between modes β and c becomes larger when $g_{bc} = 0$ compared with the case of $g_{bc} \neq 0$ [56] [evidenced by the larger frequency split of the two anticrossing modes at the resonance shown in Fig. 2(e)] and thus induces more efficient cooling of magnons [indicated by the lower population of mode β in Fig. 2(f)] as well as stronger enhancement of magnon-magnon entanglement [Fig. 2(d)]. Similar enhancement is observed when $g_{ac} = 0$.

We point out that the enhancement of the magnon-magnon entanglement appears only in the deep strong-coupling regime ($g_{ab} \sim \omega_{a,b}$), and it is absent in the weak-coupling regime and even in the strong-coupling where $g_{ab} \sim 0.01 - 0.1\omega_{a,b}$. It is clearly seen from Fig. 3(a) that in the strong-coupling regime, $g_{ab}/H_{\text{ex}} = 0.01$, the entanglement between a and c starts to appear when g_{mp} increases from its $g_{\text{mp}} = 0$ value, whereas the entanglement between a and b slightly decreases. This is expected since part of the entanglement between a and b is transferred to mode c through the beam-splitter-type coupling between modes b and c. On the other hand, in the case of the deep strong-coupling regime illustrated in Fig. 3(b) for $g_{ab}/H_{\text{ex}} = 1.0$, significant enhancement of the magnon-magnon entanglement appears, and it remains large when g_{mp} is increased [57], whereas the entanglement between a and c is completely suppressed. When the coupling strength g_{mp} is further increased such that it approaches the value of g_{ab}, the competition starts, and the entanglement between a and c appears as well, as indicated in Fig. 3(b). A complete phase diagram of these two cases is shown in Fig. 3(c). The absence of the enhancement of the magnon-magnon entanglement in the weak- and strong-coupling regimes can be well understood in the cavity-cooling scheme. In the strong-coupling regime, the entanglement between a and b without the light mode is given by $E_N \approx \ln[1 + g_{ab}/(H_{\text{ex}} + H_{\text{an}})] \approx g_{ab}/(H_{\text{ex}} + H_{\text{an}})$, which is almost equal to the entanglement of the joint vacuum $|2\theta| \approx |\tanh 2\theta| = g_{ab}/(H_{\text{ex}} + H_{\text{an}})$ since $|2\theta| \ll 1$. Hence, the cooling of the magnon mode to its vacuum does not induce considerable enhancement of the magnon-magnon entanglement, while the competition of creating entanglement between a and c reduces the original entanglement between a and b.

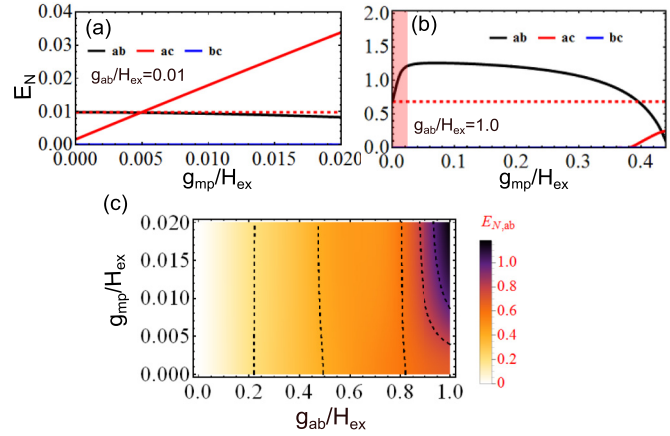

FIG. 3. The entanglement as a function of magnon-photon coupling strength g_{mp} when the system is (a) in the strong-coupling regime $g_{ab}/H_{\text{ex}} = 0.01$ and (b) in the deep strong-coupling regime $g_{ab}/H_{\text{ex}} = 1$. The red dashed lines represent the magnon-magnon entanglement in the absence of the photon mode. $\gamma_{\text{m}} = 0.001H_{\text{ex}}$, $\gamma_c = 0.003H_{\text{ex}}$. (c) The steady magnon-magnon entanglement distribution in the $g_{ab} - g_{\text{mp}}$ phase plane. The right side marks the deep strong-coupling regime, where considerable enhancement is observed. Other parameters are $H/H_{\text{sp}} = 0.15$, $\omega_c/H_{\text{sp}} = 0.85$, $\gamma_{\text{m}} = 0.001H_{\text{ex}}$, $\gamma_c = 0.003H_{\text{ex}}$.

To identify the magnon-magnon entanglement as well as the magnon-polariton near the anticrossing, the coupling strength of the magnon and photon is essentially stronger than the dissipation rate of the system ($g_{\text{mp}} > \gamma_m, \gamma_c$); otherwise, the noise will smear out the anticrossing [14]. Then it is meaningful to study the influence of the dissipation rate on the entanglement enhancement. Figure 4(a) shows the magnon entanglement as a function of γ_m. For $g_{\text{mp}}/H_{\text{ex}} = 0.01$, the entanglement keeps decreasing with γ_{m} and saturates at the value without photons (red dashed line). For $\gamma_{\text{m}} < g_{\text{mp}}$, the enhancement is always there. At a given γ_{m}, the enhancement increases with the coupling strength of magnon-photon g_{mp}. When we tune the dissipation rate of the cavity, there exists an optimized γ_c where the entanglement enhancement reaches a maximum, as shown in Fig. 4(b). The peak position falls into the regime $\gamma_c < g_{\text{mp}}$, such that the anticrossing spectrum can be identified and it is feasible to observe the magnon-polariton and the enhancement of magnon-magnon entanglement simultaneously.

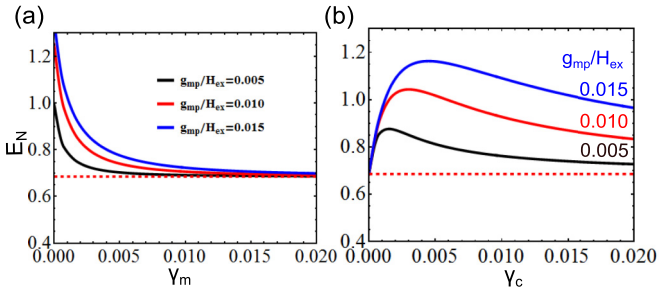

FIG. 4. (a) The entanglement of a and b as a function of the dissipation rate of magnons at the resonant condition. $g_{ab} = H_{ex}$, $H_{an} = 0.0163H_{ex}$, $\gamma_c/H_{ex} = 0.003$. (b) The entanglement of a and b as a function of the dissipation rate of photons. $H/H_{sp} = 0.15$, $\omega_c/H_{sp} = 0.85$, $\gamma_m/H_{ex} = 0.001$.

IV. DISCUSSION AND CONCLUSIONS

Ferrimagnetic/ferromagnetic case. For a two-sublattice ferrimagnet ($S_a \neq S_b$, $g_{ac} \neq g_{bc}$), the enhancement of magnon-magnon entanglement is found to be similar to that in the antiferromagnetic case, once the deep strong-coupling condition is satisfied, i.e., $g_{ab} \sim \omega_a, \omega_b$. A ferromagnet corresponds to the limiting case of $S_a \to 0$ in which $g_{ab} \propto S_a S_b \to 0$, so that the physics becomes different. Specifically, for a single sublattice ferromagnet coupled with the light mode, Eq. (5) is reduced to

$$\mathcal{H} = \omega_b b^\dagger b + \omega_c c^\dagger c + g_{bc}(b^\dagger c + b c^\dagger), \tag{10}$$

which in the case of mode b representing a set of spins corresponds to that of the Tawis-Cummings model. The spectrum of the Hamiltonian (10) takes the form $\omega_{1,2} = \frac{1}{2}[(\omega_b + \omega_c) \pm \sqrt{(\omega_b - \omega_c)^2 + g_{bc}^2}]$, which has an anticrossing near the point $\omega_b = \omega_c$.

Recently, Soykal and Flatté [27] demonstrated that the Hamiltonian (10), which describes the interaction between magnon and photons in a ferromagnet, has eigenstates corresponding to entangled states of spin orientation and photon number. These states oscillate periodically with the Rabi frequency determined by g_{bc} and can live for a long time due to a small decoherence present in the system. Since the dissipation of the modes is ignored, no steady state can be achieved. Therefore, we would like to point out that the mechanism of the creation of entangled states in the ferromagnet, as described by the Hamiltonian (10), is different from what we have used to study the steady-state entanglement in a dissipative antiferromagnet. The reason is that we have considered the dynamics of the system under the influence of a Gaussian noise, which is completely different from that determined by the Hamiltonian (10). Two modes influenced by the Gaussian noise can decay to a steady entangled state only if these modes are coupled to each other through the parametric-type interaction [51,58,59]. Thus, the presence of the parametric-type interaction between the modes is essential for getting the steady-state entanglement in a dissipative system.

Experimental verification. First, we emphasize that the essential physics of entanglement enhancement is quite robust for many realistic antiferromagnets such as diphenylpicrylhydrazyl (DPPH), MnF_2, $NaNiO_2$, and NiO (see Appendix D for the detailed simulation results). This makes our theory more relevant to experimentalists. Second, to measure the entanglement, one may place a low-damping AFM into a high-quality cavity/coplanar waveguide and measure the quadrature components of the covariance matrix of the system. The beam-splitter coupling of photons and acoustic magnons in Eq. (9) enables the readout of magnon information by inputting another weak microwave into the magnet and then homodyning the output of the probe field. Alternatively, one may use femtosecond optical pulses to pump the correlations of magnons and then measure the noise level of the system by a second probe pulse [60].

Potential applications of the hybrid system. First, since the magnons are the macroscopic excitation of a magnet, the entanglement of magnons provides a promising platform to study macroscopic quantum phenomena such as the entanglement properties of massive objects and the transition between quantum and classical phenomena. Note that the entanglement presented here is much larger and is stabler than those achieved through the nonlinear effect [21,41]; hence, our proposal gives a lot room to realize, detect, and use the entanglement. On the more practical side, (1) the entangled magnon-pair can be used to test Bell's inequality and thus the nonlocal feature of quantum mechanics. This adds another freedom to control the entanglement in the hybrid system. (2) The entangled state is also useful as a resource for minimum channel discrimination to distinguish the supremacy of channels with entangled states over those with separable states. (3) Similar to the importance of generation of high-quality entangled photons, electrons, and quasiparticles in quantum communication, quantum computation, and quantum information [61–63], magnons may also find a role in these quantum tasks for the advantage of automatically stability, deep strong entanglement, and easy tunability of magnon dispersions [64]. The manipulation of magnon entanglement by tuning anisotropy or magnetic fields was theoretically demonstrated [65]. The concept of stimulated Raman adiabatic passage for efficient and selective transfer of the population between quantum states was recently realized in magnonic systems [64].

Second, the magnon-polariton in the antiferrimagnet-light system can be classified into a wide context of cavity spintronics, aiming to manipulate quantum information with the hybrid magnon-photon state. The coupling of magnons and photons can be promisingly used as quantum transducers, quantum sensors, quantum memories, and so on [19–22]. If one aims to achieve coherent information transfer between magnons and photons, their beam-splitter-type interaction is sufficient. To illustrate this point, we propose a potential application of magnon-photon coupling as a platform to realize the state transfer between cavity photons and magnons by simply scanning the external fields.

The Hamiltonian we considered is a modified version of Eq. (9),

$$\mathcal{H} = \omega_\beta \beta^\dagger \beta + \omega_c c^\dagger c + g_{\beta c}(\beta c^\dagger + \beta^\dagger c),$$

where we disregard the high-frequency terms for its off resonance. In general, the β mode can also be the superposed magnon mode in antiferromagnets or the Kittel mode in a normal ferromagnet. The sweeping of the field will modulate ω_β and thus lead to the state evolution of the system. Without

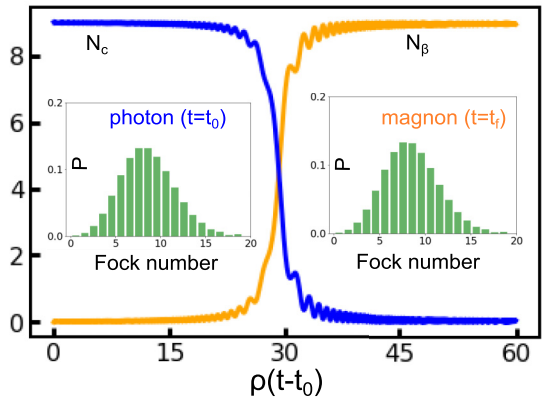

FIG. 5. Particle number occupation as a function of time. The left and right insets show the initial and final particle distributions in Fock space, respectively. The initial state is a tensor product of coherent photons and zero-occupied magnons. $g_{\beta c} = 0.02\omega_c$, $\rho = 0.01\omega_c$.

loss of generality, we consider a linear time dependence of ω_β, i.e., $d\omega_\beta/dt = \rho$, and simulate the dynamics of the system by solving the Schrödinger equation, as shown in Fig. 5. Clearly, the initial photon state at $t = t_0$ is completely transferred to the magnon states at $t = t_f$ as we sweep the field, while the particle number distribution is perfectly preserved. This process resembles the Landau-Zener transition [66,67], which was originally proposed for state evolution in a system with energy level repulsion. Since this application is not the focus of the current work, we leave a more thorough study of this transfer process to the future.

Conclusions. In summary, we have studied the entanglement properties of magnons and photons inside a cavity and find that the steady entanglement between magnons and photons is very weak. Instead, the magnons excited on the two sublattices of an AFM are strongly entangled, and this entanglement can be enhanced to its maximum when the magnons are coupled to the photon in the resonant condition. The maximum enhancement increases monotonically with the coupling strength between magnons and photons, while it optimizes at a particular dissipation rate of the cavity. We ascertain that such enhancement comes from the cavity cooling effect and is a unique feature of the antiferromagnet with the deep strong coupling between two magnons, and it disappears for a normal system with strong coupling. On the other hand, the enhanced entanglement of the magnons through cavity photons is always accompanied by better cooling of their populations. Then one can make use of the cavity photons as a resource to cool the magnons to their lower-energy states. Last, the two magnon modes and one photon mode form a closed loop in our hybrid system. By modifying the phase of the photon field (i.e., $c \to ce^{i\phi}$), the entanglement of the magnon modes can also be manipulated.

Note added. Recently, we become aware of a relevant work that reported magnon-magnon entanglement in antiferromagnets [68].

ACKNOWLEDGMENTS

H.Y.Y. acknowledges the financial support from National Natural Science Foundation of China (NSFC) Grant No. 61704071. Q.Y.H acknowledges NSFC Grants (No. 11622428, No. 61675007, and No. 11975026) and Beijing Natural Science Foundation (Grant No. Z190005). M.-H. Y. acknowledges the NSFC Grants (No. 11875160 and No. U1801661), the Key-Area Research and Development Program of Guangdong Province (Grant No. 2018B030326001), the Natural Science Foundation of Guangdong Province (Grant No. 2017B030308003), the Guangdong Innovative and Entrepreneurial Research Team Program (Grant No. 2016ZT06D348), the Science, Technology and Innovation Commission of Shenzhen Municipality (Grant No. JCYJ20170412152620376, No. JCYJ20170817105046702, and No. KYTDPT20181011104202253), the Economy, Trade and Information Commission of Shenzhen Municipality (Grant No. 201901161512).

APPENDIX A: CLASSIFICATION OF THE THREE COUPLING REGIMES

Here, we analytically show how the relative magnitude of the coupling strength g_{ab} and intrinsic frequency $\omega_{a(b)}$ can lead to a distinguishable phase of entanglement properties of a and b.

Let us start from the standard 2×2 block form of the two-mode covariance matrix,

$$\mathbf{V} = \begin{pmatrix} \mathbf{A} & \mathbf{C} \\ \mathbf{C}^T & \mathbf{B} \end{pmatrix} = \begin{pmatrix} \Lambda_a & 0 & \Lambda_c & \Lambda_d \\ 0 & \Lambda_a & \Lambda_d & -\Lambda_c \\ \Lambda_c & \Lambda_d & \Lambda_b & 0 \\ \Lambda_d & -\Lambda_c & 0 & \Lambda_b \end{pmatrix}. \tag{A1}$$

Then the two symplectic invariants can be evaluated as $\sum(\mathbf{V}) = \det \mathbf{A} + \det \mathbf{B} - 2 \det \mathbf{C}$, and $\det(\mathbf{V})$ is the determinant of $\mathbf{V}$[49,51].

For the antiferromagnetic case we studied here, the parameters are

$$\begin{aligned} &\omega_a = H_{\rm ex} + H_{\rm an} + H,\ \omega_b = H_{\rm ex} + H_{\rm an} - H, \\ &\gamma_a = \gamma_b = \gamma_m,\ g_{ac} = g_{bc} = 0. \end{aligned} \tag{A2}$$

Then the elements of the covariance matrix can be evaluated as

$$\begin{aligned} \Lambda_a = \Lambda_b &= \frac{1}{2}\left(1 + \frac{g_{ab}^2}{(H_{\rm ex} + H_{\rm an})^2 - g_{ab}^2 + \gamma_m^2}\right), \\ \Lambda_c &= -\frac{1}{2}\frac{g_{ab}(H_{\rm ex} + H_{\rm an})}{(H_{\rm ex} + H_{\rm an})^2 - g_{ab}^2 + \gamma_m^2}, \\ \Lambda_d &= -\frac{1}{2}\frac{g_{ab}\gamma_m}{(H_{\rm ex} + H_{\rm an})^2 - g_{ab}^2 + \gamma_m^2}. \end{aligned} \tag{A3}$$

Then we have

$$\begin{aligned} \sum(\mathbf{V}) &= \det \mathbf{A} + \det \mathbf{B} - 2 \det \mathbf{C} \\ &= \frac{1}{2}\frac{\left[(H_{\rm ex} + H_{\rm an})^2 + \gamma_m^2\right]\left[(H_{\rm ex} + H_{\rm an})^2 + g_{ab}^2 + \gamma_m^2\right]}{(H_{\rm ex} + H_{\rm an})^2 - g_{ab}^2 + \gamma_m^2}, \\ \mathrm{Det}(\mathbf{V}) &= \frac{1}{16}\left(\frac{(H_{\rm ex} + H_{\rm an})^2 + \gamma_m^2}{(H_{\rm ex} + H_{\rm an})^2 - g_{ab}^2 + \gamma_m^2}\right)^2, \end{aligned} \tag{A4}$$

TABLE I. Entanglement properties of modes a and b in the three distinguishable coupling regimes.

	Regime		
	Strong	Ultrastrong	Deep strong
Definition	$g_{ab} \sim 0.01 H_{\rm ex}$	$g_{ab} \sim 0.1 H_{\rm ex}$	$g_{ab} \sim H_{\rm ex}$
E_N	~0.01	~0.1	ln 2
Enhanced?	No	No	Yes

and the smallest symplectic eigenvalue

$$\eta^- = \sqrt{\sum(\mathbf{V}) - \left[\sum(\mathbf{V})^2 - 4\det\mathbf{V}\right]^{1/2}}/\sqrt{2} = \frac{1}{2}\frac{1}{1 + g_{ab}/\sqrt{(H_{\rm ex}+H_{\rm an})^2+\gamma_m^2}}. \quad \text{(A5)}$$

Then the entanglement is quantified as

$$E_N = -\ln(2\eta^-) = \ln\left(1 + \frac{g_{ab}}{\sqrt{(H_{\rm ex}+H_{\rm an})^2+\gamma_m^2}}\right). \quad \text{(A6)}$$

Now we can classify two limiting phases: (1) In the deep strong-coupling regime, i.e., $g_{ab} \sim H_{\rm ex} \gg H_{\rm an}, \gamma_m$, we have $E_N \approx \ln 2 = 0.6931$. (2) In the strong-coupling regime, i.e., $g_{ab} \ll H_{\rm ex}$, the leading-order contribution to the entanglement is $E_N \approx g_{ab}/(H_{ex}+H_{an}) \to 0$. The phase diagram is summarized in Table I.

APPENDIX B: STABILITY REGIME

To obtain the stability regime of the magnon-photon system, we numerically solve the eigenequation $\det(\lambda\mathbf{I}-\mathbf{M}) = 0$ and show the results in Fig. 6(a). The system is always stable for $g_{\rm mp} < 0.3$, which is well satisfied using realistic parameters of cavity and magnets [14]. As a comparison, we disregard the self-energy terms ($\omega_a = \omega_b = \omega_c = 0$), as adopted in many studies on quantum optics, and find that the system cannot reach a steady state in exactly the same phase space, as shown in Fig. 6(b). This comparison shows that our magnon-light system has an almost generic stability condition.

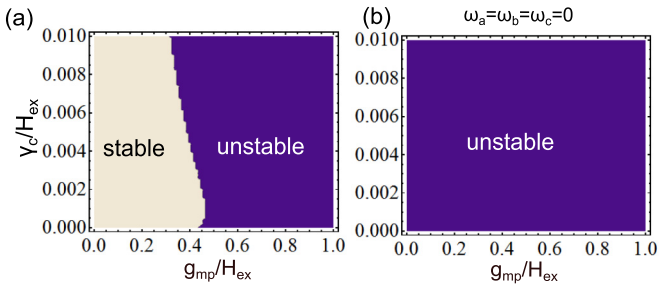

FIG. 6. (a) The stability regime of the magnon-photon system with $g_{ab} = H_{\rm ex}$, $H_{\rm an} = 0.0163 H_{\rm ex}$, $H/H_{\rm sp} = 0.15$, $\omega_c/H_{\rm sp} = 0.85$, $\gamma_{\rm m}/H_{\rm ex} = 0.001$. (b) The stability regime when the self-energy terms are disregarded, i.e., $\omega_a = \omega_b = \omega_c = 0$.

APPENDIX C: ENTANGLEMENT FOR A TWO-MODE SQUEEZED STATE

For a two-mode squeezed state defined as

$$|r\rangle = \exp\left[r\left(a_i^\dagger a_j^\dagger - a_i a_j\right)\right]|0\rangle_i \bigotimes |0\rangle_j, \; r \in \text{reals}, \quad \text{(C1)}$$

the covariance matrix is

$$\mathbf{V} = \begin{pmatrix} \mathbf{A} & \mathbf{C} \\ \mathbf{C}^T & \mathbf{B} \end{pmatrix} = \frac{1}{2}\begin{pmatrix} \cosh 2r & 0 & \sinh 2r & 0 \\ 0 & \cosh 2r & 0 & -\sinh 2r \\ \sinh 2r & 0 & \cosh 2r & 0 \\ 0 & -\sinh 2r & 0 & \cosh 2r \end{pmatrix}. \quad \text{(C2)}$$

Then we can derive

$$\sum(V) = \det\mathbf{A} + \det\mathbf{B} - 2\det\mathbf{C} = \frac{1}{2}\cosh 4r, \quad \text{(C3)}$$

$$\mathrm{Det}(V) = \frac{1}{16}, \quad \text{(C4)}$$

and the smallest symplectic eigenvalue

$$\eta^- = 2^{-1/2}\left\{\sum(\mathbf{V}) - \left[\sum(\mathbf{V})^2 - 4\det\mathbf{V}\right]^{1/2}\right\}^{1/2} \quad \text{(C5)}$$

$$= \frac{1}{2}[\cosh 4r - (\cosh^2 4r - 1)]^{1/2} \quad \text{(C6)}$$

$$= \frac{1}{2}e^{-2|r|}. \quad \text{(C7)}$$

Then the entanglement can be quantified as $E_N = -\ln(2\eta^-) = 2|r|$.

APPENDIX D: SIMULATION RESULTS FOR MORE ANTIFERROMAGNETS

In this Appendix, we examine our results by using experimental values of the parameters of the DPPH material as well as of commonly used antiferromagnets such as MnF_2, $NaNiO_2$, and NiO. The values of the parameters are listed in Table II. Here, the exchange field and the anisotropy field depend on the magnetic parameters such as $H_{\rm ex} = 2zJS^2$ and $H_{\rm an} = 2KS^2$, with K being the anisotropy coefficient. Values of both $H_{\rm ex}$ and $H_{\rm an}$ of these materials were experimentally determined through the magnetic resonance technique [15,69–71]. According to the values of these parameters, $H_{\rm an} < 0.1 H_{\rm ex}$, while the external field is of the order of $0.2 H_{\rm sp} < 0.1 H_{\rm ex}$ and is also much smaller than the exchange field $H_{\rm ex}$. Therefore, the frequencies $\omega_{a,b} = H_{\rm ex} + H_{\rm an} \pm H \approx$

TABLE II. List of parameter values used in the simulation. The exchange field of DPPH is estimated from its Néel temperature. The damping rate of MnF_2 is estimated from the linewidth measured in the experiments [69].

Material	$H_{\rm ex}(T)$	$H_{\rm an}/H_{\rm ex}$	$g_{\rm mp}/H_{\rm ex}$	$\gamma_m/H_{\rm ex}$	$\gamma_c/H_{\rm ex}$
DPPH [15]	1.73	0.018	8×10^{-4}	1.05×10^{-5}	6.12×10^{-4}
MnF_2 [69]	51.5	0.0163	0.001	9.7×10^{-6}	6×10^{-4}
$NaNiO_2$ [70]	4.8	0.073	0.012	0.001	0.005
NiO [71]	524	0.0028	3×10^{-4}	5×10^{-4}	10^{-4}

$H_{ex} = g_{ab}$, i.e., the magnon-magnon coupling strength, fall into the deep strong-coupling regime, so that our generic model presented in the main text applies to these materials. Moreover, the coupling strength of DPPH is determined by the size of the anticrossing gap observed in experiments [15], while the calculations of the values of the coupling strength with photons of the other AFMs are based on the formula $g_{mp} = \sqrt{\mu_0 \omega_c S N / 2V}$, as derived above Eq. (4), by considering that 1% of the volume of the cavity is occupied by the magnet [72]. The damping rates of the AFMs are estimated from the linewidth of the magnets [71], while the values of the damping rates of the cavity modes are consistent with the experimental values of Ref. [15].

Using these values of the parameters, we find that the enhancement of the magnon-magnon entanglement is still valid, as shown in Fig. 7. The enhancement is considerably large for DPPH (86%), MnF_2 (57%), and $NaNiO_2$ (45%). The limited enhancement in NiO may be due to the strong exchange field that effectively reduces the magnon-photon coupling and thus suppresses the cooling channel.

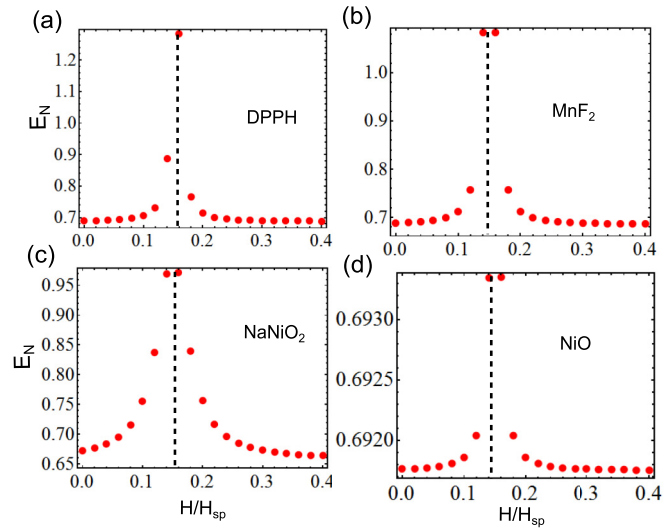

FIG. 7. (a) The entanglement of a and b as a function of external field for (a) DPPH, (b) MnF_2, (c) $NaNiO_2$, and (d) NiO. The dashed lines represent the positions of the resonance frequency.

[1] T. Jungwirth, X. Marti, P. Wadley, and J. Wunderlich, Nat. Nanotechnol. **11**, 231 (2016).

[2] V. Baltz, A. Manchon, M. Tsoi, T. Moriyama, T. Ono, and Y. Tserkovnyak, Rev. Mod. Phys. **90**, 015005 (2018).

[3] R. Cheng, J. Xiao, Q. Niu, and A. Brataas, Phys. Rev. Lett. **113**, 057601 (2014).

[4] H. Wang, C. Du, P. C. Hammel, and F. Yang, Phys. Rev. Lett. **113**, 097202 (2014).

[5] C. Hahn, G. de Liubens, V. V. Naletov, J. B. Yousser, O. Klein, and M. Viret, Europhys. Lett. **108**, 57005 (2014).

[6] W. Lin, K. Chen, S. Zhang, and C. L. Chien, Phys. Rev. Lett. **116**, 186601 (2016).

[7] L. Frangou, S. Oyarzun, S. Auffret, L. Vila, S. Gambarelli, and V. Baltz, Phys. Rev. Lett. **116**, 077203 (2016).

[8] S. Takei, B. I. Halperin, A. Yacoby, and Y. Tserkovnyak, Phys. Rev. B **90**, 094408 (2014).

[9] W. Yuan, Q. Zhu, T. Su, Y. Yao, W. Xing, Y. Chen, Y. Ma, X. Lin, J. Shi, R. Shindou, X. C. Xie, and W. Han, Sci. Adv. **4**, eaat1098 (2018).

[10] R. Lebrun, A. Ross, S. A. Bender, A. Qaiumzadeh, L. Baldrati, J. Crammer, A. Brataas, R. A. Duine, and M. Kläui, Nature (London) **561**, 222 (2018).

[11] E. G. Tveten, A. Qaiumzadeh, and A. Brataas, Phys. Rev. Lett. **112**, 147204 (2014).

[12] W. Yu, J. Lan, and J. Xiao, Phys. Rev. B **98**, 144422 (2018).

[13] H. Yang, H. Y. Yuan, M. Yan, H. W. Zhang, and P. Yan, Phys. Rev. B **100**, 024407 (2019).

[14] H. Y. Yuan and X. R. Wang, Appl. Phys. Lett. **110**, 082403 (2017).

[15] M. Mergenthaler, J. Liu, J. J. Le Roy, N. Ares, A. L. Thompson, L. Bogani, F. Luis, S. J. Blundell, T. Lancaster, A. Ardavan, G. A. D. Briggs, P. J. Leek, and E. A. Laird, Phys. Rev. Lett. **119**, 147701 (2017).

[16] K. Grishunin, T. Huisman, G. Li, E. Mishma, T. Rasing, A. V. Kimel, K. Zhang, Z. Jin, S. Cao, W. Ren, G.-H. Ma, and R. V. Mikhaylovskiy, ACS Photonics **5**, 1375 (2018).

[17] J. Everts, G. G. G. King, N. Lambert, S. Kocsis, S. Rogge, and J. J. Longell, arXiv:1911.11311.

[18] J. Clarke and M. R. Vanner, Quantum Sci. Technol. **4**, 014003 (2019).

[19] Y.-P. Wang, G.-Q. Zhang, D. Zhang, T.-F. Li, C.-M. Hu, and J. Q. You, Phys. Rev. Lett. **120**, 057202 (2018).

[20] R. Hisatomi, A. Osada, Y. Tabuchi, T. Ishikawa, A. Noguchi, R. Yamazaki, K. Usami, and Y. Nakamura, Phys. Rev. B **93**, 174427 (2016).

[21] Z. Zhang, M. O. Scully, and G. S. Agarwal, Phys. Rev. Research **1**, 023021 (2019).

[22] D. Lachance-Quirion, Y. Tabuchi, A. Gloppe, K. Usami, and Y. Nakamura, Appl. Phys. Express **12**, 070101 (2019).

[23] Y. Tabuchi, S. Ishino, A. Noguchi, T. Ishikawa, R. Yamazaki, K. Usami, and Y. Nakamura, Science **349**, 405 (2015).

[24] D. Lachance-Quirion, Y. Tabuchi, S. Ishino, A. Noguchi, T. Ishikawa, R. Yamazaki, and Y. Nakamura, Sci. Adv. **3**, e1603150 (2017).

[25] W. Yu, J. Wang, H. Y. Yuan, and J. Xiao, Phys. Rev. Lett. **123**, 227201 (2019).

[26] M. Piani and J. Watrous, Phys. Rev. Lett. **102**, 250501 (2009).

[27] Ö. O. Soykal and M. E. Flatté, Phys. Rev. Lett. **104**, 077202 (2010).

[28] Ö. O. Soykal and M. E. Flatté, Phys. Rev. B **82**, 104413 (2010).

[29] H. Huebl, C. W. Zollitsch, J. Lotze, F. Hocke, M. Greifenstein, A. Marx, R. Gross, and S. T. B. Goennenwein, Phys. Rev. Lett. **111**, 127003 (2013).

[30] Y. Tabuchi, S. Ishino, T. Ishikawa, R. Yamazaki, K. Usami, and Y. Nakamura, Phys. Rev. Lett. **113**, 083603 (2014).

[31] X. Zhang, C.-L. Zou, L. Jiang, and H. X. Tang, Phys. Rev. Lett. **113**, 156401 (2014).

[32] L. Bai, M. Harder, Y. P. Chen, X. Fan, J. Q. Xiao, and C.-M. Hu, Phys. Rev. Lett. **114**, 227201 (2015).

[33] M. Tavis and F. W. Cummings, Phys. Rev. **170**, 379 (1968).

[34] A. Retzker, E. Solano, and B. Reznik, Phys. Rev. A **75**, 022312 (2007).

[35] C. E. López, F. Lastra, G. Romero, and J. C. Retamal, Phys. Rev. A **75**, 022107 (2007).

[36] A. Dehghani, B. Mojaveri, S. Shirin, and S. A. Faseghandis, Sci. Rep. **6**, 38069 (2016).

[37] S. Agarwal, S. M. H. Rafasanjani, and J. H. Eberly, Phys. Rev. A **85**, 043815 (2012).

[38] M. Harder, L. Bai, C. Match, J. Sirker, and C.-M. Hu, Sci. China Phys. Mech. Astron. **59**, 117511 (2016).

[39] M. Harder, Y. Yang, B. M. Yao, C. H. Yu, J. W. Rao, Y. S. Gui, R. L. Stamps, and C.-M. Hu, Phys. Rev. Lett. **121**, 137203 (2018).

[40] D. Lachance-Quirion, S. P. Wolski, Y. Tabuchi, S. Kono, K. Usami, and Y. Nakamura, arXiv:1910.09096.

[41] J. Li, S.-Y. Zhu, and G. S. Agarwal, Phys. Rev. Lett. **121**, 203601 (2018).

[42] J. Li and S.-Y. Zhu, New J. Phys. **21**, 085001 (2019).

[43] H. Y. Yuan, P. Yan, S. Zheng, Q. Y. He, K. Xia, and M.-H. Yung, arXiv:1905.11117.

[44] H. Y. Yuan and M.-H. Yung, Phys. Rev. A **98**, 022125 (2018).

[45] H. Y. Yuan and M.-H. Yung, Phys. Rev. B **97**, 060405(R) (2018).

[46] T. Holstein and H. Primakoff, Phys. Rev. **58**, 1098 (1940).

[47] D. F. Walls and G. J. Milburn, *Quantum Optics*, 2nd ed. (Springer, Berlin, 2008).

[48] In general, $\langle c_{\rm in}(t)c_{\rm in}^{\dagger}(t')\rangle = (n_{\rm th}+1)\delta(t-t')$, where $n_{\rm th}$ is the Bose-Einstein distribution function for the photons. Here, we consider the low-temperature case such that $n_{\rm th} \ll 1$, and we choose $n_{\rm th} = 0$.

[49] D. Vitali, S. Gigan, A. Ferreira, H. R. Bohm, P. Tombesi, A. Guerreiro, V. Vedral, A. Zeilinger, and M. Aspelmeyer, Phys. Rev. Lett. **98**, 030405 (2007).

[50] E. X. DeJesus and C. Kaufman, Phys. Rev. A **35**, 5288 (1987).

[51] G. Adesso and F. Illuminati, J. Phys. A **40**, 7821 (2007).

[52] In Ref. [51], the logarithmic negativity is $E_N = \max[0, -\ln(\nu^-)]$.This difference comes from the missing $\sqrt{2}$ in the definition of the quadratures, which results in a prefactor 2 difference of the covariance matrix and the consequent symplectic eigenvalue $\nu^- = 2\eta^-$.

[53] C. Genes, A. Mari, P. Tombesi, and D. Vitali, Phys. Rev. A **78**, 032316 (2008).

[54] S. L. Braunstein and P. van Loock, Rev. Mod. Phys. **77**, 513 (2005).

[55] Y.-D. Wang and A. A. Clerk, Phys. Rev. Lett. **110**, 253601 (2013).

[56] Here, the absolute value of $g_{\beta c}$ matters since the effective coupling, i.e., the width of the gap at the anticrossing, is related to $g_{\beta c}^2$. See Ref. [14] for more details.

[57] Here, the essential physics of the enhancement of magnon-magnon entanglement is insensitive to the value of $g_{\rm mp}$ in the deep strong-coupling regime. To achieve strong enhancement, one can use a magnet with a reasonably large number of spins to enhance the coupling strength $g_{\rm mp}$, as shown in Appendix D, while the optical power is not necessarily large in this process such that the nonlinear effect originating from the spin-orbital coupling can be suppressed.

[58] Q. Y. He and Z. Ficek, Phys. Rev. A **89**, 022332 (2014).

[59] X. Huang, E. Zeuthen, Q. Gong, and Q. Y. He, Phys. Rev. A **100**, 012318 (2019).

[60] J. Zhao, A. V. Bragas, D. J. Lockwood, and R. Merlin, Phys. Rev. Lett. **93**, 107203 (2004).

[61] J. Liu, R. Su, Y. Wei, B. Yao, S. F. C. da Silva, Y. Yu, J. Iles-Smith, K. Srinivasan, A. Rastelli, J. Li, and X. Wang, Nat. Nanotechnol. **14**, 586 (2019).

[62] O. A. Castro-Alvaredo, C. De Fazio, B. Doyon, and I. M. Szécsényi, Phys. Rev. Lett. **121**, 170602 (2018).

[63] P. Samuelsson, E. V. Sukhorukov, and M. Büttiker, New J. Phys. **7**, 176 (2005).

[64] K. Bergmann, H.-C. Nägerl, C. Panda, G. Gabrielse, E. Miloglyadov, M. Quack, G. Seyfang, G. Wichmann, S. Ospelkaus, A. Kuhn, S. Longhi, A. Szameit, P. Pirro, B. Hillebrands, X.-F. Zhu, J. Zhu, M. Drewsen, W. K. Hensinger, S. Weidt, T. Halfmann, H. Wang, G. S. Paraoanu, N. V. Vitanov, J. Mompart, Th. Busch, T. J. Barnum, D. D. Grimes, R. W. Field, M. G. Raizen, E. Narevicius, M. Auzinsh, D. Budker, A. Pálffy, and C. H. Keitel, J. Phys. B: At. Mol. Opt. Phys. **52**, 202001 (2019).

[65] J. Zou, S. K. Kim, and Y. Tserkovnyak, arXiv:1909.09653.

[66] L. D. Landau, Phys. Z. Sowjetunion **2**, 46 (1932).

[67] C. Zener, Proc. R. Soc. London, Ser. A **137**, 696 (1932).

[68] A. Kamra, E. Thingstad, G. Rastelli, R. A. Duine, A. Brataas, W. Belzig, and A. Sudbø, Phys. Rev. B **100**, 174407 (2019).

[69] J. P. Kotthaus and V. Jaccarino, Phys. Rev. Lett. **28**, 1649 (1972).

[70] E. Chappel, M. D. Nez-Regueiro, F. Dupont, G. Chouteau, C. Darie, and A. Sulpice, Eur. Phys. J. B **17**, 609 (2000).

[71] T. Moriyama, K. Hayashi, K. Yamada, M. Shima, Y. Ohya, and T. Ono, Phys. Rev. Materials **3**, 051402(R) (2019).

[72] Ø. Johansen and A. Brataas, Phys. Rev. Lett. **121**, 087204 (2018).